

Cracking the Puzzle of CO₂ Formation on Interstellar Ices

Quantum Chemical and Kinetic Study of the CO + OH → CO₂ + H Reaction.

G. Molpeceres¹, J. Enrique-Romero², and Y. Aikawa¹

¹ Department of Astronomy, Graduate School of Science, The University of Tokyo, Tokyo 113 0033, Japan
e-mail: molpeceres@astron.s.u-tokyo.ac.jp

² Leiden Institute of Chemistry, Gorlaeus Laboratories, Leiden University, PO Box 9502, 2300 RA Leiden, The Netherlands
e-mail: j.enrique.romero@lic.leidenuniv.nl

Received July 11, 2023; accepted July 11, 2023

ABSTRACT

Context. CO₂ is one of the dominant components of the interstellar ice. Recent observations show CO₂ exists more abundantly in polar (H₂O-dominated) ice than in apolar (H₂O-poor) ice. CO₂ ice formation is primarily attributed to the reaction between CO and OH, which has a barrier.

Aims. We investigate the title reaction in H₂O ice and CO ice to quantify the efficiency of the reaction in polar ice and apolar ice.

Methods. Highly accurate quantum chemical calculations were employed to analyze the stationary points of the potential energy surfaces of the title reaction in the gas phase on a H₂O and CO clusters. Microcanonical transition state theory was used as a diagnostic tool for the efficiency of the reaction under ISM conditions. We simulate the kinetics of ice chemistry, considering different scenarios involving non-thermal processes and energy dissipation.

Results. The CO + OH reaction proceeds through the remarkably stable intermediate HOCO radical. On the H₂O cluster, the formation of this intermediate is efficient, but the subsequent reaction leading to CO₂ formation is not. Conversely, HOCO formation on the CO cluster is inefficient without external energy input. Thus, CO₂ ice cannot be formed by the title reaction alone either on H₂O cluster or CO cluster.

Conclusions. In the polar ice, CO₂ ice formation is possible via CO + OH → HOCO, followed by HOCO + H → CO₂ + H₂, as demonstrated by abundant experimental literature. In apolar ice, CO₂ formation is less efficient because HOCO formation requires external energy. Our finding is consistent with the JWST observations. Further experimental work is encouraged using low-temperature OH radicals.

Key words. ISM: molecules – Molecular Data – Astrochemistry – methods: numerical

1. Introduction

In the cold molecular clouds of the interstellar medium (ISM), a significant fraction of the molecules are contained in the solid phase in the form of ice. While most of the molecules present in the ISM have been detected in the gas phase using radio telescopes through their rotational transitions, the direct observation of ices requires studying their vibrational transitions, which are commonly affected by telluric contamination. In this context, space telescopes, such as Spitzer or, more recently, JWST, are essential. Ice observations Öberg et al. (2011); Boogert et al. (2015); McClure et al. (2023) reveal the presence of several components such as H₂O, CO, CH₃OH, and the object of this study, CO₂. The abundance of these species, as well as their speciation in the ice or their presence in specific regions of the ISM, can only be explained by considering their formation routes and the chemical conditions necessary for their appearance.

The different components of interstellar ice may be formed in situ on the surface of refractory material. Such is the case of H₂O, which is formed from the hydrogenation of atomic oxygen (Ioppolo et al. 2008; Dulieu et al. 2010; Lamberts et al. 2014, 2013; Meisner et al. 2017; Molpeceres et al. 2019), or the case of CH₃OH, which is formed from the hydrogenation of CO (Watanabe & Kouchi 2002; Fuchs et al. 2009; Rimola et al. 2014). Other

significant components are primarily synthesized in the gas and accrete under extremely cold and dense conditions on the grain, like CO. Interstellar carbon dioxide, CO₂, is thought to form via reactions on the surface (see, e.g., Garrod & Pauly (2011); Pauly & Garrod (2018)). The postulated reactions contributing to the CO₂ formation are:



From this ternary of reactions, Reaction 3 has a barrier energy when atomic oxygen is in its ground state, (³P)O (Minissale et al. 2013). Reaction 2 is barrierless, and Reaction 1, the reaction whose study we tackle in this paper, is assumed to have a minimal activation energy (~ 100 K, Garrod & Pauly (2011)).

The assumption of tiny activation energy for the CO + OH → CO₂ + H reaction is supported by a plethora of experiments dealing with surface chemical experiments (Ioppolo et al. 2011; Noble et al. 2011; Oba et al. 2010a,b; Qasim et al. 2019; Gutiérrez-Quintanilla et al. 2021; Terwisscha van Scheltinga et al. 2022). Each of these experiments vary in different factors, including the formation route of the OH radical, either by

hydrogenation of O_2 , (Ioppolo et al. 2011; Noble et al. 2011; Qasim et al. 2019), dissociation of H_2O molecules before deposition on the ice (Oba et al. 2010a,b), or direct photodissociation of H_2O molecules (Terwisscha van Scheltinga et al. 2022). Other variations between experiments include the substrate under consideration, either amorphous silicates (Noble et al. 2011), CO (Qasim et al. 2019), matrix isolation Gutiérrez-Quintanilla et al. (2021) or H_2O (Ioppolo et al. 2011; Oba et al. 2010a,b; Terwisscha van Scheltinga et al. 2022). On the modelling side, Garrod & Pauly (2011) build on the experimental knowledge and coarse-grained it in a combination of a direct formation route $CO+OH \longrightarrow CO_2+H$ operating at $T \geq 12$ K, coinciding with the onset of CO diffusion on H_2O , and an indirect three-body route on CO ices that relies in the formation of a kinetically excited OH radical $O + H \longrightarrow OH^*$ that subsequently partakes in the $CO+OH^*$ reaction. The latter route on CO ices allows to explain the CO_2 bands in a non-polar media observed in infrared observations of ices (Öberg et al. 2011; Boogert et al. 2015; McClure et al. 2023). In summary, there is ample evidence for Reaction 1, to be efficient on dust grains. However, the same reaction in the gas phase is relatively slow, with rate constants as low as $\sim 2 \times 10^{-13}$ molecules $cm^{-3} s^{-1}$ at 300 K (Frost et al. 1991). The title reaction in the gas phase has also been a source of extensive theoretical attention. It has been simulated using both semi-classical and quantum dynamics on highly accurate potential energy surfaces (PES) (Ma et al. 2012; Caracciolo et al. 2018; Li et al. 2014). It was also studied in the presence of other CO_2 molecules Masunov et al. (2018). The theoretical works find rate constants even lower than the values reported in Frost et al. (1991).

The different reactivity on surfaces and the gas phase is puzzling and counterintuitive. In both phases, the reaction is acknowledged to proceed through the highly stable HOCO radical. The evolution from this radical is the primary source of uncertainty because of the high activation energies to form the bimolecular $CO_2 + H$ products. In the gas, where a third body to stabilize HOCO is unavailable, the reaction is more likely to occur owing to the energy redistribution into the few vibrational degrees of freedom, ultimately leading to an irreversible reaction. On the surface, the ice molecules dissipate a significant fraction of this energy, ideally leading to the thermalization of HOCO, hence slowing or impeding the formation of CO_2 . This was proved by Arasa et al. (2013), initiating the conundrum we tackle in this work and that has also been debated from different prisms (Bredehöft 2020; Upadhyay et al. 2021; Tachikawa 2021). If the reaction is slow in the gas, it should not proceed on the ice, where little energy is left for the reaction after dissipation into the ice. Hence, how is the mismatch between gas and solid phase experiments possible? In this article, we aim to shed light on this particular issue. The two main possibilities to explain the disagreement include, in the first place, the operation of external energy input, either chemical from the $O_2 + H$ or $O + H$ reactions required to form the OH radical, or the excess energy used to photodissociate H_2O . Secondly, free H atoms from the experiment may promote H abstraction reactions, $HOCO + H \longrightarrow CO_2 + H_2$. While these two possibilities are often assumed when interpreting the experimental results, it is fundamental to distinguish which is dominant, if any, to establish under which conditions the laboratory measurements apply to the ISM. Determining the factors contributing to the reaction yield in the experiments is complicated because the detection techniques are suited for identifying only the final products. Quantum chemical calculations are instrumental and provide an atomistic perspective of the different elementary processes relevant to the reaction.

In this work, we simulate the title reaction on two different model ices, H_2O and CO, and perform kinetic simulations using a microcanonical formalism to determine the importance of non-thermal effects in the reaction, including dissipation over different numbers of molecules, and complete the picture left by the different experimental studies. The paper is structured as follows. In Section 2, we describe the employed computational methodology. In Section 3 we present the structural models for the ices (Section 3.1), the PES for the reactions in each of the surfaces (Section 3.2 and Section 3.2.2) and the associated kinetic analysis (Section 3.3). Section 4 is dedicated to interpreting our results from an astrophysical point of view, contextualising the preceding experiments. We finally summarize our main findings in Section 5.

2. Methodology

2.1. Quantum chemical calculations

The stationary points in the PES were characterized using density functional theory (DFT) calculations on model clusters mimicking H_2O and CO ices. Because this work aims to determine the impact of energy redistribution in the formation of CO_2 on ice, we need to use sufficiently large structural models to allow for (ergodic) energy equipartition. In a preceding calculation, Rimola et al. (2018) used a cluster containing 33 H_2O water molecules and discussed the suitability of a model of this size, indicating that energy dissipation should be well described with a model of this size. This was later confirmed with dedicated studies using ab-initio molecular dynamics simulations (Pantaleone et al. 2021, 2020; Ferrero et al. 2023; Molpeceres et al. 2023b). Therefore, in this study, we use the same 33 H_2O cluster to simulate the H_2O ice (Rimola et al. 2018), and we constructed a 33 CO cluster to simulate the CO ice. To construct such a cluster, we used PACKMOL (Martinez et al. 2009) in a 8 Å radius sphere, ensuring that every molecule is at a minimum initial distance of 3 Å from each other. This initial cluster is later refined at the level of the theory described below.

The geometries of the initial clusters were optimized at the MN15-D3BJ/6-31+G(d,p) level of theory (Yu et al. 2016; Grimme et al. 2010, 2011; Hehre et al. 1972; Hariharan & Pople 1973; Ditchfield et al. 1971; Clark et al. 1983), with parameters for the D3BJ dispersion correction taken from Goerigk et al. (2017). The DFT and optimizations utilize the GAUSSIAN16 (rev.C.01) suite of programs (Frisch et al. 2016). We later place the CO and OH admolecules on the clusters sequentially, first occupying a binding site for the CO molecule and later for OH. Once the two admolecules are located on the clusters, we followed the gas-phase reaction mechanism presented in Ma et al. (2012) for both clusters, except for an alternative exit path on CO ice (Section 3.2.2). Additional differences between the gas-phase and surface-like profiles are highlighted in Section 3.2. After locating every stationary point, we confirmed them as either true minima or first-order saddle points, i.e., transition states (TS), in the PES by computing the molecular Hessian of the system. The electronic energies of the stationary points on the PES were further refined using the domain-based local pair-natural orbital coupled cluster singles and doubles with a perturbative treatment of triple excitations, DLPNO-CCSD(T) (Riplinger et al. 2016; Guo et al. 2018) using a two-point complete basis set extrapolation (CBS) to the basis-set limit using the cc-pVDZ and cc-pVTZ basis sets (Woon & Dunning 1993; Helgaker et al. 1997; Neese & Valeev 2011; Zhong et al. 2008; Neese et al. 2020). The internal options for the PNO localization scheme were set to

normal, and resolution of the identity (RI) techniques were used to evaluate exchange and Coulomb integrals (RIJK) using a cc-pVTZ/JK auxiliary basis set. We apply the frozen-core approximation in the correlated calculations. The ORCA (v.5.0.4) code was used for the DLPNO-CCSD(T)/CBS calculations (Neese 2012; Neese et al. 2020; Neese 2022).

In addition to cluster calculations, we also carried out gas-phase calculations at the same level of theory for comparative purposes, which are indicated throughout the paper in square brackets. Finally, we assessed the quality of our theoretical method of choice, comparing our gas phase results with the ones of Ma et al. (2012), finding excellent agreement for all the relevant parts of the PES. These results are presented in the Appendix A. It is worth noting here that our theoretical method does not predict the correct energetics for the high energy intermediate HCO₂. This intermediate is not relevant to the kinetics of the system because its formation requires surmounting an emerged barrier of ~8-9 kcal mol⁻¹ from the bimolecular OH+CO asymptote (38-39 kcal mol⁻¹ from the HOCO potential well) (Ma et al. 2012; Masunov et al. 2018). Moreover, we could not find this intermediate in the simulations on the H₂O cluster. We, therefore, skip the search for this intermediate in all cluster calculations. Nonetheless, we discuss the origin of this disagreement in Appendix A.

2.2. Kinetic Analysis

We employed the microcanonical flavour of the transition state theory, called Rice–Ramsperger–Kassel–Marcus (RRKM) to compute the energy-dependent rate constants $k(E)$ for the transitions between reaction wells, given by:

$$k(E) = \frac{N^\ddagger(E - E_0)}{h\rho(E)}, \quad (4)$$

where h is the Planck’s constant, $N^\ddagger(E - E_0)$ is the sum of states of the transition state evaluated at energy E to the energy of the transition state, E_0 , and $\rho(E)$ is the density of states of the reactant at energy E . In addition, the sum of states contains tunnelling corrections, for which the non-symmetric Eckart potential model was employed (Eckart 1930; Johnston & Heicklen 1962). We did not include rotational symmetry factors in our calculations due to the symmetry breaking induced by the amorphous surface. The rigid-rotor harmonic oscillator model is used throughout the kinetic calculations. The application of RRKM to interstellar reactions is discussed in Rimola et al. (2018) and used or implied in several other works (Enrique-Romero et al. 2021; Perrero et al. 2022; Baiano et al. 2022)

As it will be explained later on (Section 3.3), the title reaction occurs strictly non-thermally at 10 K. Hence we make our analysis based on $k(E)$ for the entrance CO + OH \longrightarrow t-HOCO/c-HOCO and exit channels: c-HOCO \longrightarrow CO₂ + H (and alternatively c-HOCO/t-HOCO + CO \longrightarrow CO₂ + HCO, Section 3.2.2). We provide $k(E)$ considering several energy dissipation scenarios. Each of them has a different number of molecules, n , over which instantaneous energy dissipation is allowed. We studied $n=16$, 10, 5, and 0 (CO/H₂O) molecules. In the latter ($n=0$), energy redistribution occurs only within the CO + OH system. We carried out this study by projecting out the molecular Hessian matrix elements for the m molecules (where $m = 33 - n$) farther from the t-HOCO minima, as the global minima of our study. The microcanonical rate constants obtained in this study are calculated with the MESS code (Georgievskii et al.

Table 1. Binding energies (ZPVE corrected, ΔU , in kcal mol⁻¹ and Kelvin, in parenthesis), of the CO and OH admolecules at the reaction site considered in this work. The binding energies of t-HOCO and c-HOCO, discussed in Section 3.2 are also included.

Adsorbate/Surface	ΔU
CO/H ₂ O	4.64 (2335)
OH/H ₂ O	6.45 (3246)
CO/CO	0.73 (367)
OH/CO	2.25 (1132)
t-HOCO/H ₂ O	14.51 (7302)
c-HOCO/H ₂ O	12.30 (6190)
t-HOCO/CO	3.52 (1771)
c-HOCO/CO	2.50 (1258)

2013). We note that the sizes of the clusters (see Figure 1) and the highest number of dissipating water molecules are sufficient according to previous studies, e.g., Pantaleone et al. (2020, 2021). Although no specific studies have addressed this issue for CO ice, we have made a reasonable assumption that the same holds true. It is worth highlighting again that we considered different dissipating CO ice molecules.

3. Results

3.1. Cluster model

The fully optimized H₂O and CO clusters mimicking ice surfaces are presented in Figure 1. While the CO ice model has a more spherical and compact shape with dimensions 10×12×13 Å, the water one is slightly more elongated, 15×9×10.5 Å. The latter hosts a cavity, where the CO+OH \longrightarrow CO₂+H reaction is simulated. On the contrary, the more compact CO cluster does not have any clear deeper binding site. Hence the reaction site was randomly chosen.

The binding energies of the reactants and reaction intermediates on the surfaces are presented in Table 1. These were calculated as the energy difference between the complexes containing the surface and the admolecule and the sum of the isolated fragments, including ZPVE. In the H₂O cluster cavity, we find a binding energy for CO of 4.64 kcal mol⁻¹, higher than the values reported by Ferrero et al. (2020) (≤ 3.71 kcal mol⁻¹). This indicates that our cavity is a really deep binding site with a maximized number of neighbour water molecules. For the OH radical, on the contrary, the cavity binding site yields lower than average binding energies (6.45 kcal mol⁻¹) than other reported values, e.g., 10.33 kcal mol⁻¹ (Duflo et al. 2021), and 10.6 kcal mol⁻¹ (Enrique-Romero et al. 2022). The observed differences arise from the specific structure of our cavity, where the number of dangling H-bonds is saturated, and the binding mode of OH, whose acceptor/donor H-bonds about 0.1 Å shorter than in the cavity case reported by Enrique-Romero et al. (2022). On the CO cluster, the CO/CO binding energy corresponds to the lower bound of the values presented in Ferrari et al. (2023) while the values of OH/CO are unreported. We note that the dual-level error introduced by our calculations is relevant for determining binding energies for CO/CO due to the mismatch of geometries arising from the weak CO-CO interaction in the ice (Ferrari et al. 2023). In the subsequent reactivity studies, the relative magnitude of this error is diminished because energy differences between reaction steps are much higher than the CO-CO interaction energy.

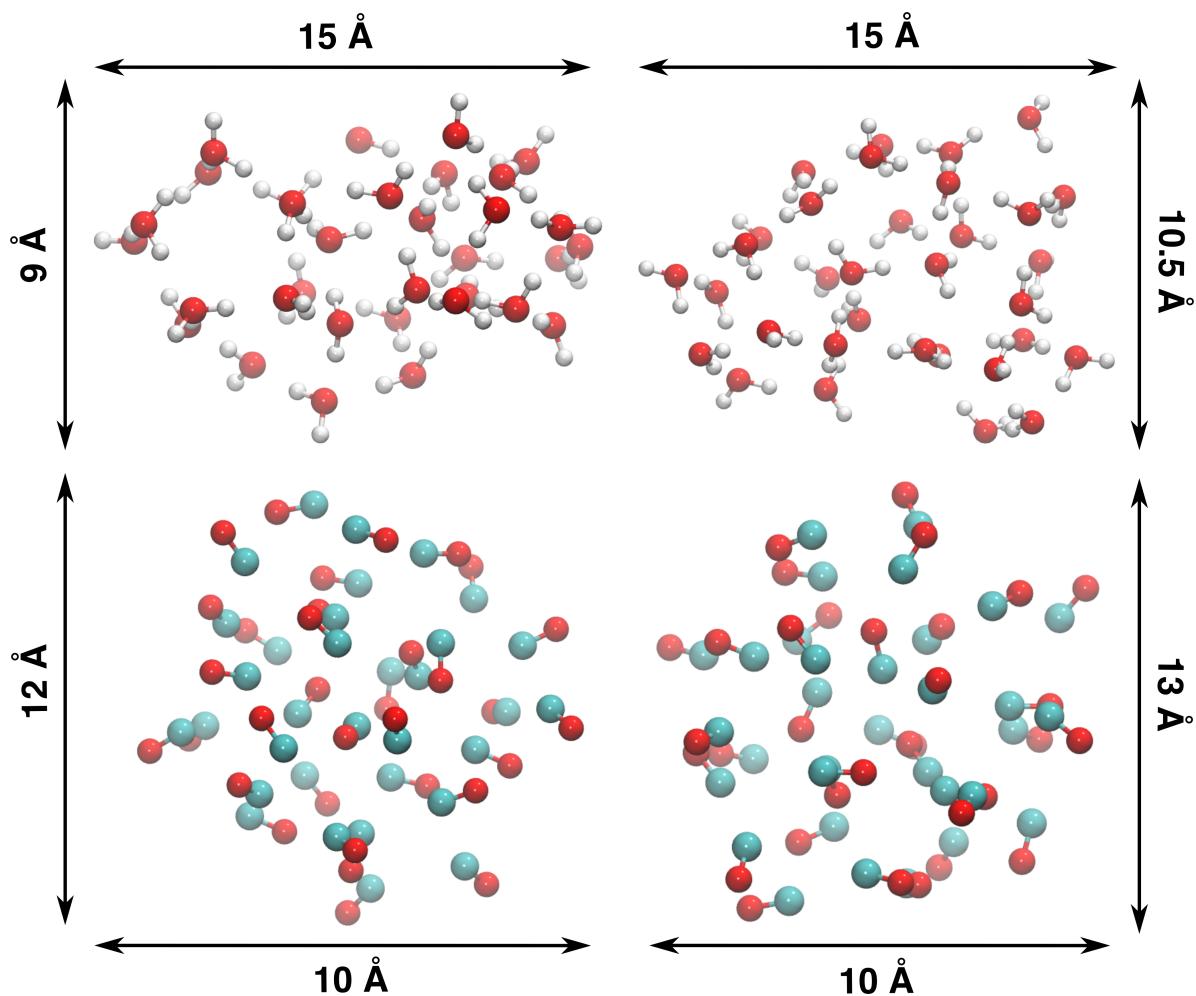


Fig. 1. Views of the clusters employed to simulate the $\text{CO} + \text{OH} \longrightarrow \text{CO}_2 + \text{H}$ reaction. **Top Left-** Side view of the H_2O ice cluster. **Top Right-** Top view of the H_2O ice cluster. **Bottom Left-** Side view of the CO ice cluster. **Bottom Right-** Top view of the CO ice cluster. Color code: White-Hydrogen, Red-Oxygen, Teal-Carbon. The size of the clusters is determined approximately by measuring the cluster's endpoints.

For the reactivity studies, we keep the CO binding site determined above, while the OH radical is placed on a different binding site. We justify this choice based on two arguments. First, when both adsorbates are thermalized, the higher interstellar abundance of CO makes it more likely to be located in deep binding sites, such as the cavity formed in the H_2O cluster. Second, in Section 3.3, we investigate the effect of a translationally excited OH radical colliding with a pre-adsorbed CO.

3.2. Potential energy surface construction

All the energy diagrams have been referenced from the asymptotes, i.e., from the sum of energies of the surface, reacting CO and the reacting OH radical. We will refer to this as the bimolecular system, and for the sake of simplicity it will be denoted as CO + OH, regardless of the ice surface. This was done for the sake of clarity, as it is much clearer what the influence of the substrate in stabilizing the reactants is, as well as its catalytic effect on the barriers.

3.2.1. H_2O ice

We include two pre-reactant complexes following the literature (Ma et al. 2012; Masunov et al. 2018). First, a pre-reactant complex with large dihedral $\angle\text{HOCO}$ angles, PRC, which leads to the

formation of the t-HOCO intermediate. Second, a near 0° dihedral angle pre-reactant complex (PRC'), that forms the c-HOCO intermediate (which was not found on CO ice, as discussed in Section 3.2.2). The transition states that connect the PRCs with the reaction wells are named TS1 and TS1', respectively, and the transition state connecting these two wells is TS2. Finally, the transition state leading to $\text{CO}_2 + \text{H}$ from c-HOCO is named TS4. The reason for not naming it TS3 is that the TS3 label (specifically TS3') is reserved for the exit transition state from t-HOCO, a stationary point we do not find on water ice.

The stationary points on the reaction profile are gathered in Figure 2. The reaction profile has, for the most part, the same profile as in the gas phase, with two notable exceptions. The first concerns the absence of the HCO_2 intermediate, as we already discussed in Section 2.1. The second is the inversion in energy between PRC and PRC'. This inversion appears following the formation of a $\text{HO}\cdots\text{H}_2\text{O}$ hydrogen bond that locks the PRC' geometry in the binding site contiguous to the CO binding site. The snapshots of the stationary points are collated in Figure 3, where this effect can be visualized. The higher stabilization of PRC' also results in higher activation energy to c-HOCO through TS1'.

The binding energies of t-HOCO and c-HOCO on the cavity are $15.51 \text{ kcal mol}^{-1}$ (7805 K) and $12.30 \text{ kcal mol}^{-1}$ (6190 K), respectively. These binding energies are significantly higher

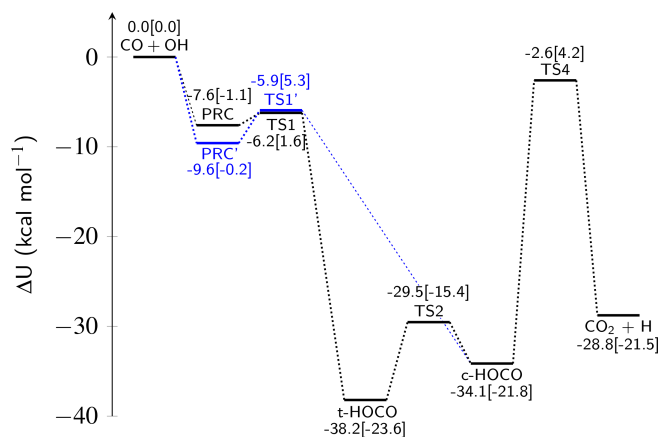


Fig. 2. Reaction profile for the $\text{CO} + \text{OH} \longrightarrow \text{CO}_2 + \text{H}$ reaction on the ASW cluster. Energies are referred to as the sum of the isolated components, e.g. CO, OH, $(\text{H}_2\text{O})_{33}$. In square brackets, the energies for the gas-phase reaction. All energies are ZPVE corrected.

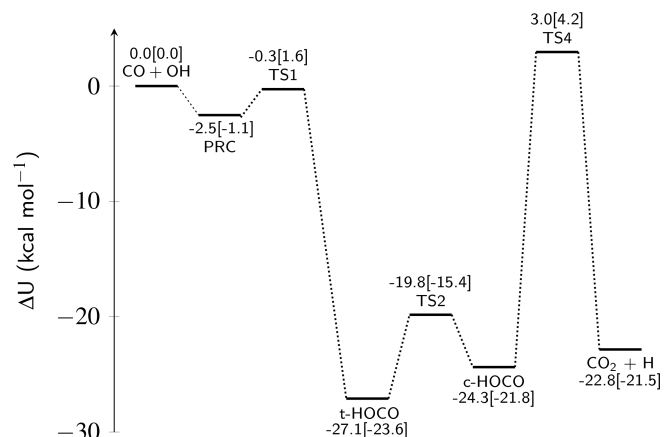


Fig. 4. Reaction profile for the $\text{CO} + \text{OH} \longrightarrow \text{CO}_2 + \text{H}$ reaction on the amorphous CO cluster. Energies are referred to as the sum of the isolated components, e.g. CO, OH, $(\text{CO})_{33}$. In square brackets, the energies for the gas-phase reaction. All energies are ZPVE corrected.

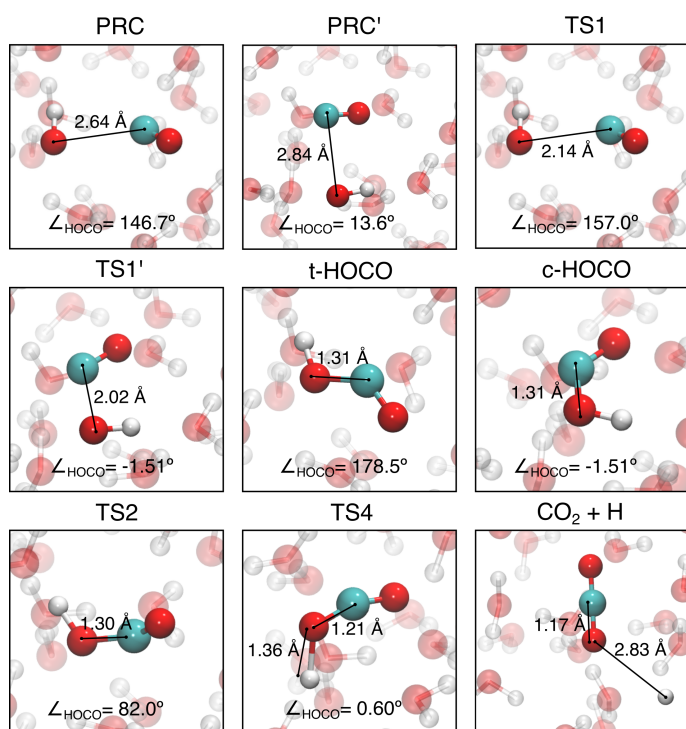


Fig. 3. Stationary points on the $\text{CO} + \text{OH} \longrightarrow \text{CO}_2 + \text{H}$ reaction profile for the reaction on top of the $(\text{H}_2\text{O})_{33}$ cluster. For all the intermediates and transition states we indicate the value of the dihedral angle $\angle\text{HOCO}$ governing the isomerism of the t-HOCO and c-HOCO wells. Color code. White-Hydrogen, Red-Oxygen, Teal-Carbon.

than the ones for CO and OH presented in Table 1, and are closer to the average values reported for the related molecule, HC(O)OH, formic acid (e.g., $\sim 12.30 \text{ kcal mol}^{-1}$ Molpeceres, G. et al. (2022), $10.7\text{--}21.0 \text{ kcal mol}^{-1}$ Ferrero et al. (2020)). The t-HOCO and c-HOCO wells are significantly stabilized on the surface, evinced by the $13\text{--}16 \text{ kcal mol}^{-1}$ difference in energy with the same intermediates in the gas phase. As a consequence, the activation energy of TS4 is higher on water. When breaking the O–H bond in c-HOCO, the energy corresponding to the OH moiety must be overcome, i.e. a significant fraction of the binding energy. The binding energy of the $\text{CO}_2 + \text{H}$ system on H_2O was found to be $7.30 \text{ kcal mol}^{-1}$ (3673 K).

Finally, from Figure 2, it is evident that the reaction, if viable, must proceed through quantum tunnelling. The $\text{c-HOCO} \longrightarrow \text{CO}_2 + \text{H}$ barrier is $32.1 \text{ kcal mol}^{-1}$, which is extremely high for ISM conditions. However, contrary to what happens in the gas phase, TS4 is submerged with respect to the reactant asymptote, thanks to the stabilization promoted by the H_2O surface. The product of the reaction, $\text{CO}_2 + \text{H}$, is higher in energy than both radicals, and the reaction is significantly less exothermic because of the break of hydrogen bonds. Nonetheless, once $\text{CO}_2 + \text{H}$ is formed, H is susceptible of diffusing or evaporating, thus concluding the reaction.

3.2.2. CO ice

The reaction profile on CO ice is shown in Figure 4 and the stationary points in Figure 5. With respect to the gas-phase process, as previously discussed, the profile lacks the HCO₂ intermediate. When comparing with the results for the water cluster presented above, the main difference is the lack of PRC', so that the reaction must go through the t-HOCO intermediate to reach CO_2 . While PRC' exists on the CO ice, we found it to be a first-order saddle point. Unlike in water, where PRC' is stabilized thanks to the interaction of the OH radical with a dangling bond of H_2O , on CO, this interaction is unavailable, and the weak OH-CO interaction promotes the rotation to PRC. There is still the possibility that the lack of PRC' is an effect of the random selection of the binding site, however a full binding site sampling is beyond our computational resources. To reach the t-HOCO intermediate, however, the TS1 must be crossed at the same energy level as the asymptote. Hence, significant energy dissipation would suppress the whole reaction unless enough energy input is provided via non-thermal mechanisms.

Additionally, the much reduced inter-molecular interaction of the admolecules with the surface due to the lack of electrostatic and H-bonding interactions of CO ices affects the energetics of the stationary points. The most prominent examples are the lower stabilisation of intermediates and the barrier in TS4, which sits above the energy of the asymptote. In general, the energetics on CO ice is closer to the gas phase case, with small differences, e.g., the isomerisation barrier for the $\text{t-HOCO} \longrightarrow \text{cis-HOCO}$ reaction on CO is about 1 kcal mol^{-1} lower (and about 2 kcal mol^{-1} lower for the reverse reaction).

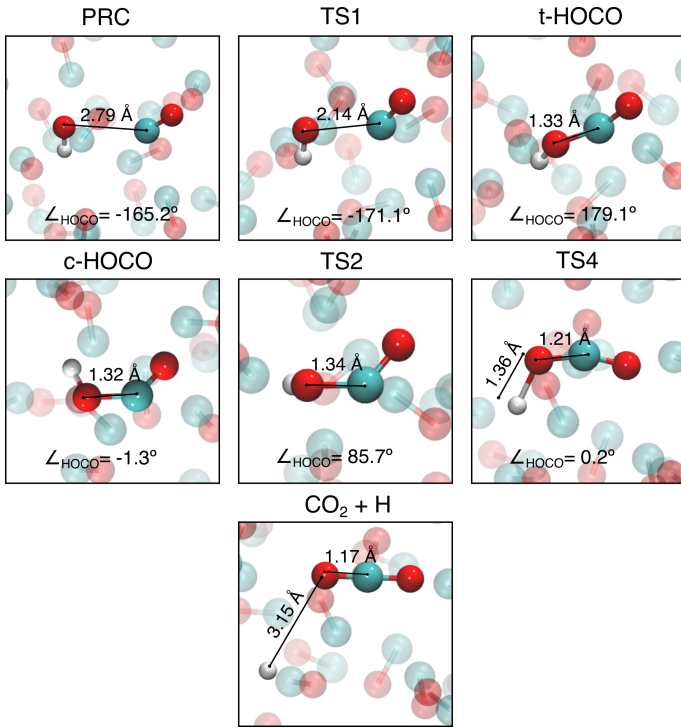


Fig. 5. Stationary points on the $\text{CO} + \text{OH} \longrightarrow \text{CO}_2 + \text{H}$ reaction profile for the reaction on top of the $(\text{CO})_{33}$ cluster. For all the intermediates and transition states we indicate the value of the dihedral angle $\angle\text{HOCO}$ governing the isomerism of the t-HOCO and c-HOCO wells. Color code. White-Hydrogen, Red-Oxygen, Teal-Carbon.

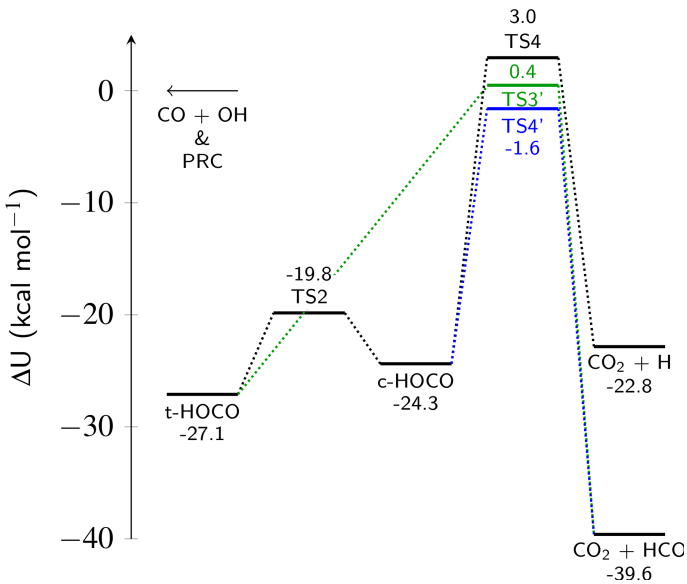


Fig. 6. Reaction profile for the $\text{CO} + \text{OH} \longrightarrow \text{CO}_2 + \text{H}$ and $2\text{CO} + \text{OH} \longrightarrow \text{CO}_2 + \text{HCO}$ alternative reaction on the amorphous CO cluster. Energies are referred to as the sum of the isolated components, e.g. CO , OH , $(\text{CO})_{33}$. Note that we omit the separated reactants asymptote and prc energies, already presented in Figure 4. All energies are ZPVE corrected.

The fact that there are more CO molecules surrounding the reaction site opens a new possibility not available on water ice or the gas phase. It involves the reactivity of the t-HOCO and cis-HOCO intermediates with a neighbouring CO, leading to $\text{CO}_2 + \text{HCO}$, see Figure 7. Interestingly, these reactions possess lower activation energy barriers than TS4, see Figure 6, and in

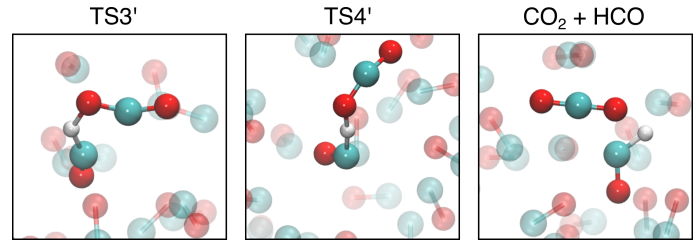


Fig. 7. Additional stationary points to the ones presented in Figure 5 for the alternative reaction channel $2\text{CO} + \text{OH} \longrightarrow \text{CO}_2 + \text{HCO}$. Color code. White-Hydrogen, Red-Oxygen, Teal-Carbon.

the case of the cis-HOCO + $\text{CO} \longrightarrow \text{CO}_2 + \text{HCO}$ reaction, the barrier sits below the asymptote.

3.3. Microcanonical rate constants

We estimated the microcanonical rate constants for the PES entrance and exit channels described in the previous sections. The entrance channels start with the pre-reactant complexes and finish with t/c-HOCO, and the exit channels start with t/c-HOCO and finish with $\text{CO}_2 + \text{H}$, and additionally $\text{CO}_2 + \text{HCO}$ for CO. These channels present the relevant rate constants for the kinetics of the reaction because the t-HOCO \longrightarrow c-HOCO is much faster, even when energy redistribution is at play. Notice that due to the barriers (TS1 and TS1'), if the stationary points of the PES were populated according to a thermal distribution, the formation of the HOCO intermediates would be slow, and the formation of products would likely not happen at all. To simulate non-thermal reactions, an initial amount of energy is given to the system; see below. Experiments of Oba et al. (2010b) show the formation of HOCO with an apparent small barrier or null barrier. We note that for the exit channel (c/t)-HOCO \longrightarrow $\text{CO}_2 + \text{H}/\text{HCO}$, the starting potential well is very deep, and thermalization is more likely (Arasa et al. 2013). Nevertheless, as we will show, under a microcanonical formalism, the formation of $\text{CO}_2 + \text{H}$ is found to be slow. Finally, different energy dissipation is allowed by changing the number of ice molecules considered in the microcanonical calculations, n .

Our PESs indicate that adsorption energy (formation of PRC/PRC') is not completely dissipated but employed in forming HOCO. The energy reference is again the energy of the asymptotes. One could consider that this is not the best choice since the initial energy lies above the energy of the PRC/PRC' and it would actually mean that the initial state is actually higher in energy than a fully thermalized reactant set. However, it must be noted that (i) if a reference state is an upper bound of the real one, and even in this case the reaction is not plausible, then starting from a more stable reference will not change the qualitative picture, and (ii) in cases where an incomplete energy dissipation promoted by certain exothermic processes, e.g. diffusion into deeper binding sites and possible Eley-Rideal mechanisms¹ would actually involve higher initial energies than PRC/PRC'. This effect is irrelevant when the activation energy of a reaction is much higher than the exothermicity caused by the mentioned processes, but for $\text{CO} + \text{OH} \longrightarrow \text{HOCO}$ the activation energy of the reaction falls below the adsorption energy, and it is of small magnitude. The correct energy reference would lie somewhere in between that of the asymptote and the PRC/PRC'.

¹ That may be of relevance for CO molecules given their abundance in ISM ices.

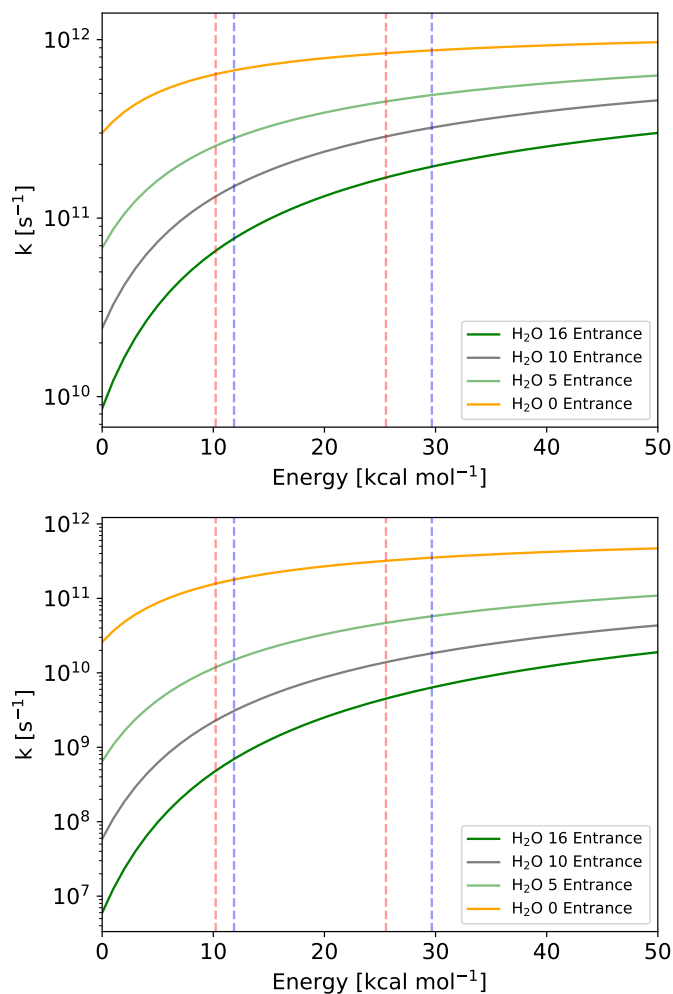


Fig. 8. Microcanonical (energy-dependent) rate constants for the $\text{CO} + \text{OH} \rightarrow \text{t-HOCO}$ (top) and $\text{CO} + \text{OH} \rightarrow \text{c-HOCO}$ (bottom) reaction step on H_2O ice. The different solid lines represent different ergodic energy dissipation scenarios, with n molecules accepting the reaction energy. The vertical dashed lines indicate fractions (0.1 and 0.25) of the $\text{O} + \text{H}$ reaction (red) and of half the energy of a Lyman alpha photon (blue); see text. The zero of energy is defined as the PES asymptote (e.g. no adsorption).

The microcanonical rate constants for the entrance step are shown in Figure 8 and Figure 9 for H_2O and CO ice. In this plot, we show the reaction rate constants as a function of the energy, where $k(E=0)$ corresponds to the separated, no adsorption asymptote ($\text{CO} + \text{OH}$ in Figure 2 and Figure 4). Energies above zero indicate extra energy from non-thermal excitation mechanisms. In this work, to compare with experimental observations, we will consider the presence of extra energy from either (i) a prior $\text{O} + \text{H} \rightarrow \text{OH}$ reaction ($\Delta U = 102.1 \text{ kcal mol}^{-1}$) or (ii) half the energy deposited by a single Ly- α photon, assuming equal energy partition into the products of the $\text{H}_2\text{O} \rightarrow \text{OH} + \text{H}$, ($\Delta U = 118.7 \text{ kcal mol}^{-1}$). Notice that the amount of extra energy used to promote the title reaction through the non-thermal mechanisms is unknown. Hence, we represent fractions of that energy, 0.10, 0.25, 0.50, as vertical dashed lines in Figure 8 and Figure 9 to serve as a guide to evaluate how the rate constants would increase under these assumed scenarios. As we introduced in Section 2, we evaluated the behaviour of the reaction assuming dissipation into a set of n molecules. The four different cases for $n=0, 5, 10, 16$ are illustrated in Figure 10 and Figure 11.

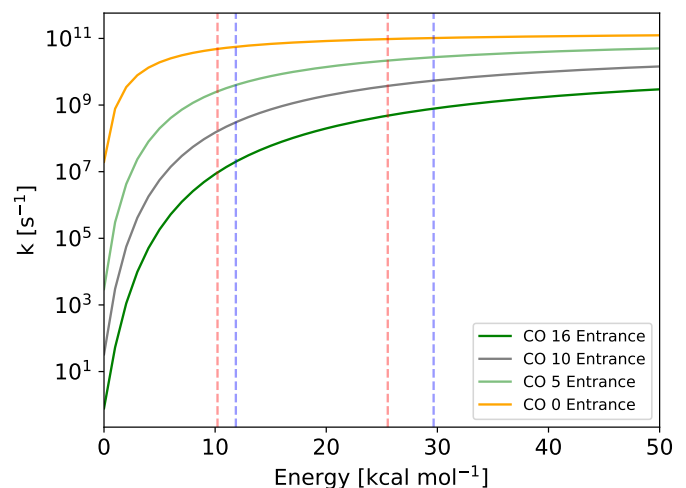


Fig. 9. Microcanonical (energy-dependent) rate constants for the $\text{CO} + \text{OH} \rightarrow \text{t-HOCO}$ reaction step on CO ice. The different solid lines represent different ergodic energy dissipation scenarios, with n molecules accepting the reaction energy. The vertical dashed lines indicate fractions (0.1 and 0.25) of the $\text{O} + \text{H}$ reaction (red) and of half the energy of a Lyman alpha photon (blue); see text. The zero of energy is defined as the PES asymptote (e.g. no adsorption).

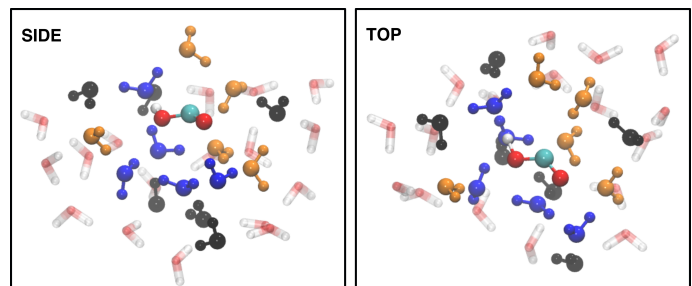


Fig. 10. Graphic representation of the different layers admitting energy dissipation through RRKM equipartition in the H_2O model ice. The t-HOCO molecule (0 dissipating molecules) is represented with red, teal and white spheres. The 5 H_2O model includes the t-HOCO molecule and H_2O molecules portrayed in blue. The 10 and 16-molecule model are represented with gold and black molecules, respectively. Finally, the rest of the molecules are represented as transparent liquorices.

The rate constants for the entrance step on H_2O ice are, for all n dissipating molecules, fast for the $\text{PRC} \rightarrow \text{t-HOCO}$ step, indicating that external energy input is unnecessary for this reaction, as determined experimentally by Oba et al. (2010b) and computationally by Arasa et al. (2013). However, for the alternative $\text{PRC}' \rightarrow \text{c-HOCO}$ reaction, we observe $k(E=0) \leq 10^8 \text{ s}^{-1}$ for the models with 10, 16 H_2O dissipating molecules. This means that if the timescale for thermalization is shorter than tens of nanoseconds, the adsorption energy alone is insufficient to overcome the entrance barrier. This constraint is lifted by considering extra energy. The reason for the difference between rate constants for the reactions starting from PRC and PRC' stems from the significantly higher activation energy in the latter case.

For the CO model, we observe systematically lower values of $k(0)$ than in water, owing to the lower stabilization of the PRC complex on CO than on H_2O leading to higher energy barriers than in the best case for H_2O . This, in turn, yields $k(E=0) \leq 10^8 \text{ s}^{-1}$ for all of our models. Because $k(E)$ is a very steep function around $E=0$, the reaction is viable with a small input of energy that can come from reactions, e.g. $\text{O}_2 + \text{H}$ (Qasim et al. 2019).

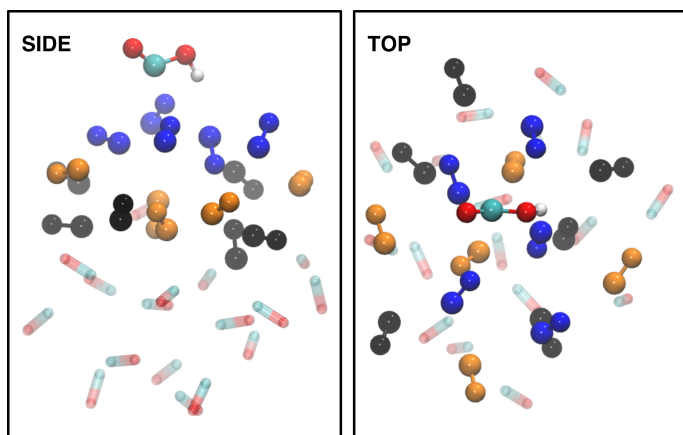


Fig. 11. Graphic representation of the different layers admitting energy dissipation through RRKM equipartition in the CO model ice. The t-HOCO molecule (0 dissipating molecules) is represented with red, teal and white spheres. The 5 CO model includes the t-HOCO molecule and CO molecules portrayed in blue. The 10 and 16-molecule model are represented with gold and black molecules, respectively. Finally, the rest of the molecules are represented as transparent liquorices.

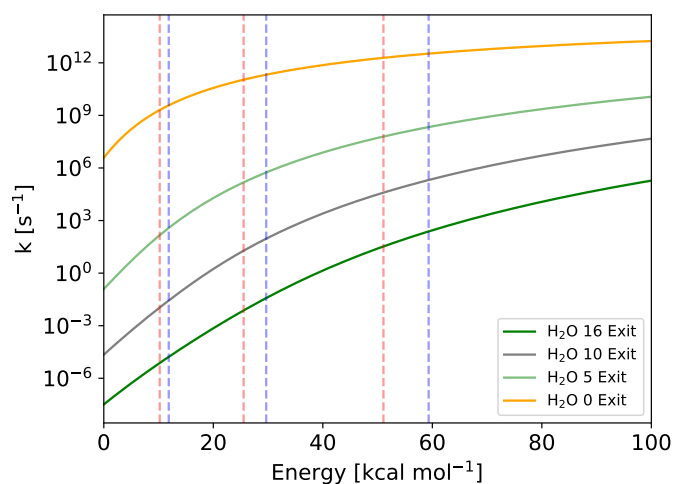


Fig. 12. Microcanonical (energy-dependent) rate constants for the $c\text{-HOCO} \rightarrow \text{CO}_2 + \text{H}$ reaction step on H_2O ice. The different solid lines represent different ergodic energy dissipation scenarios, with n molecules accepting the reaction energy. The vertical dashed lines indicate fractions (0.1, 0.25 and 0.5) of the $\text{O} + \text{H}$ reaction (red) and of half the energy of a Lyman alpha photon (blue); see text. The zero of energy is defined as the PES asymptote (e.g. no adsorption).

This finding reinforces the scenario presented in Garrod & Pauly (2011) for the three body formations of CO_2 on CO ice, as we will discuss in Section 4. An important comment for each of these rate constants is that we implicitly assumed an infinitely fast energy partition into n molecules, which may not be a good representation of this reaction on CO. At this research stage, we warn that extracting strong conclusions for a limit case like the one found for $\text{PRC} \rightarrow \text{t-HOCO}$ on CO ice is difficult and more sophisticated approaches are necessary. We are currently working on a molecular dynamics study of this reaction to illuminate this issue.

Similarly to the entrance rate constants, the exit $c\text{-HOCO} \rightarrow \text{CO}_2 + \text{H}$ rate constants on H_2O ice and $c/\text{t-HOCO} \rightarrow \text{CO}_2 + \text{H/HCO}$ rate constants on CO ice are plotted in Figure 12 and Figure 13 for the different dissipation

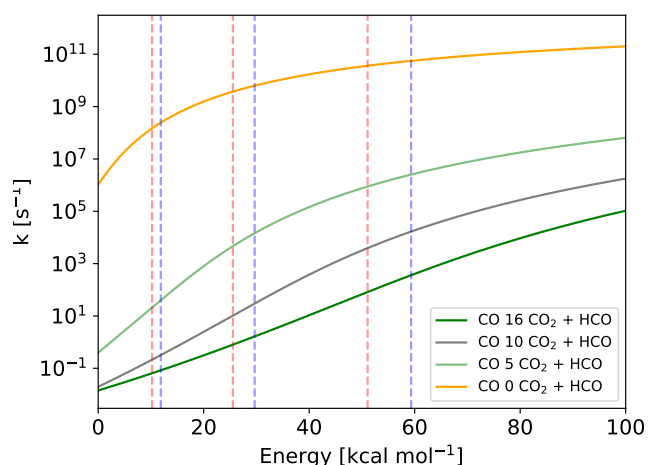
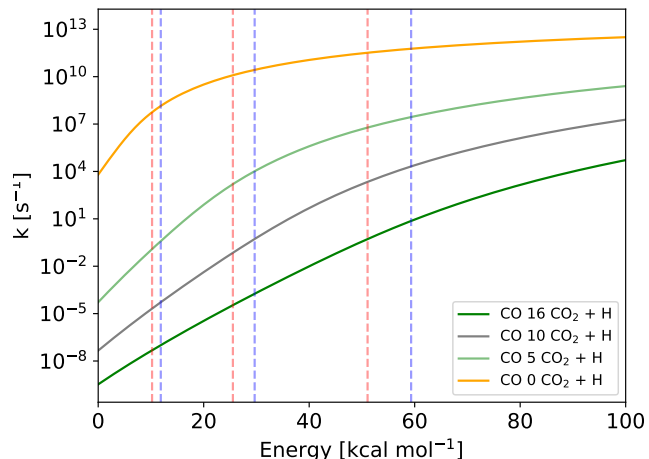
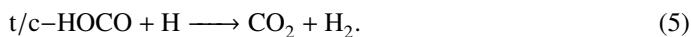


Fig. 13. Microcanonical (energy-dependent) rate constants for the $c\text{-HOCO} \rightarrow \text{CO}_2 + \text{H}$ (top) and $c\text{-HOCO} + \text{CO} \rightarrow \text{CO}_2 + \text{HCO}$ (bottom) reaction step on CO ice. The different solid lines represent different ergodic energy dissipation scenarios, with n molecules accepting the reaction energy. The vertical dashed lines indicate fractions (0.1, 0.25 and 0.5) of the $\text{O} + \text{H}$ reaction (red) and of half the energy of a Lyman alpha photon (blue); see text. The zero of energy is defined as the PES asymptote (e.g. no adsorption).

scenarios. It is important to remind that while the entrance channels are unaffected by quantum tunnelling, all the exit channels involve the migration of an H atom, turning quantum tunnelling into an important driver for the reaction, as already evinced by nuclear quantum dynamics calculations (Ma et al. 2012). Still, even with the influence of quantum tunnelling, the reactions are, in all cases, significantly slower than in the entrance step. The importance of the energy dissipation scheme is major for these reactions. There is a clear gap in exit rate constant values between the (ideal) $n=0$ dissipation model and the 5, 10 and 16 molecules dissipation models that, in all the cases, yield rate constants $k(E=0) \leq 0 \text{ s}^{-1}$. We remind that these values must be confronted against the thermalization timescale, i.e. if thermalization is faster, the reaction will not proceed. A rate constant of $k(E=0) \leq 0 \text{ s}^{-1}$ means reaction times of seconds, and we find it hard that thermalization would not happen on those timescales, precluding all the $c/\text{t-HOCO} \rightarrow \text{CO}_2 + \text{H/HCO}$ reactions in all the conditions and substrates considered in this work. We conclude then that, without the input of any external energy

other than the adsorption energy of the reactants, the reaction can proceed neither microcanonically nor from thermalized HOCO.

When including a degree of external energy from the mechanisms explained above (chemical and H₂O photodissociation), the exit reaction is faster, as expected. However, only the $n=0$ dissipation model yields rate constants that are sufficiently high $\geq 10^8 \text{ s}^{-1}$ to compete with thermalization. The upper bound of the timescale for (almost) complete thermalization of HOCO is estimated to be similar to that of CO₂ formed from the CO + (¹D)O \longrightarrow CO₂ reaction, that is, a few nanoseconds (Upadhyay et al. 2021). While the energy dissipation in RRKM is instantaneous, and an incomplete energy dissipation may increase the values of the rate constants, our assumption for the external energy input is also rather ideal. Thus, we conclude that even in the presence of external energy input, we find it hard to justify the formation of CO₂ and H/HCO from the title reaction. This suggests that the formation of CO₂ relies on the subsequent reaction described as follows:



Reaction 5 involves two radicals, and even though an activation barrier may be present on ice (Enrique-Romero et al. 2022) quantum tunnelling should play a major role, as it is the case found for H abstraction reactions (Molpeceres, G. et al. 2022; Molpeceres et al. 2023a). Thus, reaction 5 must be viable. The inclusion of reaction 5 in the CO₂ reaction network was already in place for the non-energetic formation of CO₂, for example, in Qasim et al. (2019). Still, this article shows that it also applies to the energetic formation of CO₂. We put our results in a laboratory/simulation and astrophysical context in Section 4.

Finally, and despite it does not affect the outcome of the reactions studied in this work (e.g. the $t/c\text{-HOCO} + \text{CO} \longrightarrow \text{CO}_2 + \text{H/HCO}$ reactions remain non-viable under ISM conditions), it is interesting from a purely chemical perspective to comment on the effect observed for the two competing reactions $c\text{-HOCO} \longrightarrow \text{CO}_2 + \text{H}$ and $t/c\text{-HOCO} + \text{CO} \longrightarrow \text{CO}_2 + \text{HCO}$. The competition between these two processes is energy dependent. At low values of E , e.g. $k(E = 0)$, favours $t/c\text{-HOCO} + \text{CO} \longrightarrow \text{CO}_2 + \text{HCO}$ whereas $c\text{-HOCO} \longrightarrow \text{CO}_2 + \text{H}$ is the preferred exit channel at higher energies, between 10–120 kcal mol⁻¹, depending on the number of dissipating molecules. The dependence on the energy and number of dissipating molecules clearly reveals that the dominion of the $c\text{-HOCO} \longrightarrow \text{CO}_2 + \text{H}$ route at high energies is an entropic effect. For both routes, the count of states at the TS energy (the numerator of Equation (4)) depends on the height of the barrier and the number of low-frequency vibrational modes. Because HCO, in contrast with H, has two molecular vibrations, H–C and C=O, at 2800 and 1900 cm⁻¹, the count of states will be smaller at high energies. Low-frequency vibrations overwhelm the purely kinetic effect arising from the lower barrier.

4. Discussion

4.1. The CO + OH \longrightarrow CO₂ + H reaction in the laboratory

The experiments carried out in the CO + OH \longrightarrow CO₂ + H reaction were reviewed in Section 1. For most of them, the biggest experimental conundrum is the generation of the OH radical, which is very unstable under laboratory conditions and needs to be generated in situ. The experimental methods for forming

the OH radical in these experiments are, in most cases, different. However, all the possible formation pathways involve the co-deposition or co-generation of H atoms e.g. formation with CO₂ + H, fragmentation of H₂O in a microwave discharge or H₂O photodissociation. In general, it is impossible to experimentally discern whether the CO + OH reaction proceeds directly to CO₂ + H or, in turn, stops at $t\text{-HOCO}$, which is converted to CO₂ via reaction 5.

A rigorous study of the reaction using molecular dynamics (Arasa et al. 2013) showed the probability of direct formation of CO₂ on H₂O ice is lower than 1%. It is important to remark that in Arasa et al. (2013), the OH was generated with excess energy coming from photodissociation of H₂O. Our results support the latter scenario and discard the direct reaction. Compared with our results, the small fraction observed for the direct formation of CO₂ + H in Arasa et al. (2013) may come from the slower and more realistic non-ergodic energy dissipation present in the molecular dynamics study.

On CO ice, the reaction proceeds similarly to in H₂O, both in our calculations and in the experiments of Qasim et al. (2019), where HOCO is explicitly included as the intermediate for the reaction. Qasim et al. (2019) discuss the competition with formic acid (HC(O)OH) through the reaction:



with Reaction 5. Our results complement these experiments as well, showing that in addition to what was already known, the formation of the HOCO complex has to surmount an activation energy of 2.2 kcal mol⁻¹ with a mere adsorption energy of 2.5 kcal mol⁻¹, in contrast with H₂O ice, where the higher stabilization of the PRC complex increases the energetic budget for the formation of HOCO. The consequence of this effect in the overall reaction scheme is that the formation of HOCO cannot be taken for granted on CO ice under a non-energetic regime. In Qasim et al. (2019), such energy input is given by a preceding chemical reaction. The more impeded formation of the HOCO radical on CO is the main difference with H₂O ice and is illustrated by the rate constants in Figure 8 (Top panel) and Figure 9. This different reactivity on different substrates may explain the recent JWST observations of a higher degree of mixing of CO₂ with H₂O than with CO (McClure et al. 2023). However, and as we indicated in section Section 3.3, further studies are being undertaken to understand the precise behaviour of the CO + OH \longrightarrow $t\text{-HOCO}$ association step on CO ices.

On the other hand, Gutiérrez-Quintanilla et al. (2021) used matrix isolation, electron paramagnetic resonance and FT-IR techniques, which made it possible to observe several radicals, among which HOCO, and CO₂. HC(O)OH is also detected, although its formation seems to be due to HCO + OH rather than reaction 6. In this experiment, methanol molecules embedded in an Argon matrix are photolysed at 14 K. The resulting photo-products can relax as the matrix acts as a third body. Later the sample is warmed up to 35 K, and the Ar matrix is removed, allowing light species to diffuse. The peak of CO₂ production occurs in this last stage. According to our results and interpretation, if CO₂ is formed via reaction 1, either there is some extra energy input, not all the energy from the photolysis step was completely dissipated, or H-abstraction reactions are in place. In the latter case, this can be triggered by other radicals rather than reaction 5, something we did not consider in this work, and that would require either the diffusion at warmer temperatures or the presence of a nearby radical species. In addition, an efficient H-abstraction radical-radical channel should be present, which will

certainly depend on their relative orientation (Enrique-Romero et al. 2022). Notice that in this experiment, no ice surface is present, but rather the bare copper plate on top of which the matrix and reactant mixture is prepared. Finally, we would like to encourage more experiments on CO₂ formation starting from thermalized reactants, especially on CO surfaces.

4.2. The CO + OH \longrightarrow CO₂ + H reaction in the ISM

The comparison between the experiments and our calculations presented in the last section motivates us to contextualize our results in the expected conditions of the ISM. We concluded that the sole CO+OH reaction is insufficient for the formation of CO₂ on ices and that Reaction 5 is the most promising candidate for the follow-up reaction. Considering this, is it justified to consider a small activation energy for the OH + CO \longrightarrow CO₂ + H reaction in astrochemical models of molecular clouds and prestellar cores? In light of our simulations, we consider that there are at least four different cases.

1. High coverage of H₂O ice and high abundance of H atoms.
2. High coverage of H₂O ice and low abundance of H atoms.
3. High coverage of CO ice and high abundance of H atoms.
4. High coverage of CO ice and low abundance of H atoms.

On H₂O ice (Cases 1 and 2 above), the formation of the HOCO complex is facile and does not require any energy input, with a fast reaction occurring thanks to the adsorption energy (or a fraction of it) on water ice. Moreover, the dominance of H₂O in the early stages of a molecular cloud's life, during the translucent cloud phase (Snow & McCall 2006), ensure mild temperature conditions (15–50 K) that allow for diffusion of CO molecules, and relatively low extinction ($A_V \sim 1\text{--}2$ mag). Under these conditions, Case 1 is the most likely one, with H atoms produced from photodissociation of H₂O and other hydrogenated molecules both in the gas and on the grain. Other mechanisms, such as cosmic ray ionization, also contribute to these fragmentation processes. Under these conditions, we determine that considering a null or low activation barrier for Reaction 1 in astrochemical models is justified because the H atom will ensure prompt conversion of HOCO to CO₂ through reaction 5. However, we warn that HC(O)OH abundance could be underestimated following this approach. At higher extinctions, but without enough CO surface coverage (Case 2, molecular cloud stage), the abundance of H atoms on grain surfaces will be reduced, and the HOCO complex will survive longer on the grain. Under these conditions, we recommend differentiating Reaction 1 and 5.

The next two cases (Cases 3 and 4) can be treated jointly. Our simulations show that forming the HOCO radical from CO + OH is not straightforward on CO ice and requires initial energy input. While the energy required to initiate the reaction is not very high, the very low temperatures where Cases 3 and 4 would dominate (dense prestellar cores with $T=10$ K) discard the thermal energy as the initiator of the reaction. This energy input can come from a neighbouring chemical reaction because H₂O photodissociation should be a small factor in CO ices. Therefore we consider that the approach presented in Garrod & Pauly (2011) of modelling the CO₂ formation as the three-body reaction, e.g. H+O+CO is a good compromise to model the reaction on CO ice. Whether the three-body reaction can be coarse-grained to yield CO₂ + H directly or HOCO (and later proceed through reaction 5) is likely to depend on the H atom abundance. For example, an important factor should be the local cosmic ray

ionization rate (ζ) determining the dissociation of H₂ into 2H, thus the ratio of HOCO radicals to H atoms. We must emphasize that coarse-graining the formation of CO₂ through the title reaction to study CO₂ formation and evolution may be acceptable only when H atom abundance overwhelms HOCO abundance. However, in doing so, the abundance of other HOCO-derived molecules like HC(O)OH will be underestimated. Precaution is advised when the target of the models involves these molecules.

Finally we would like to discuss other possible scenarios. One possibility is that the excited formation of OH leads to non-thermal diffusion out of the reaction site or its desorption (notice that the latter would be more plausible on CO ices due to the lower binding energy), in these cases the reaction would not take place. Another possible scenario regards the energy dissipation after HOCO is formed. Because of the high exothermicity of the CO + OH \longrightarrow HOCO reaction and the low binding energies of these radicals on CO ice, there is the possibility that HOCO chemically desorbs, or triggers the desorption of a nearby ice CO molecule. In addition, if these reactions would have to take place in the inner layers of the ice, one must take into account that energy dissipation would be even more efficient due to the larger number of intermolecular interactions and the higher number of surrounding molecules, rendering each reaction step less and less efficient.

5. Conclusions

Using accurate quantum chemical calculations and microcanonical kinetic modelling, we found that the CO+OH \longrightarrow CO₂+H reaction, which has been considered as the most important producer of interstellar CO₂, is rather inefficient, and its occurrence cannot be taken for granted. The reaction proceeds through a rather stable intermediate, HOCO, and more specifically through its two structural isomers t-HOCO and c-HOCO. On H₂O ice, the formation of HOCO is feasible, but its evolution to CO₂ requires a further reaction step that most likely involves H abstraction through reaction 5. On CO ice, we found, for the first time, that the formation of HOCO is not as efficient as currently assumed, owing to the lower adsorption energy of OH and CO molecules on CO ice. We indicate that non-thermal effects are necessary to form HOCO, and thus CO₂, on CO ice. This limitation may be behind the recent ice observations showing higher fraction of CO₂ found in water-dominated environments (Boogert et al. 2015; McClure et al. 2023) when comparing with apolar (CO-dominated) ices.

Because our calculations assume an ideal energy redistribution in an infinitely short time after the reactions, our results represent a lower bound for the production of HOCO and CO₂ from the CO + OH reaction. We aim to improve the description of energy dissipation in forthcoming works to resolve ambiguous cases. We encourage further experimental work on the topic, especially on CO ices following Qasim et al. (2019). Nonetheless, with our results, we were able to provide atomistic insight into the formation of CO₂, one of the most important interstellar ice constituents, and indicate the cases where coarse-graining of the CO + OH reaction in astrochemical models is, to a first approximation, acceptable and not.

Acknowledgements. G.M. thanks the Japan Society for the Promotion of Science (JSPS International Fellow P22013, and Grant-in-aid 22F22013) for its support. The authors acknowledge support by the Research Center for Computational Science in Okazaki, Japan (Projects: 22-IMS-C301, 23-IMS-C128), the state of Baden-Württemberg through the bwHPC consortium and the German Research Foundation (DFG) through grant no INST 40/575-1 FUGG (JUSTUS 2 cluster) (Project: 22-IMS-C301). Y.A. acknowledges support by Grant-in-Aid for Transformative Research Areas (A) grant Nos. 20H05847.

References

- Arasa, C., Van Hemert, M. C., Van Dishoeck, E. F., & Kroes, G. J. 2013, *The Journal of Physical Chemistry A*, 117, 7064
- Baiano, C., Lupi, J., Barone, V., & Tasinato, N. 2022, *Journal of Chemical Theory and Computation*, 18, 3111
- Boogert, A. C., Gerakines, P. A., & Whittet, D. C. 2015, *Annual Review of Astronomy and Astrophysics*, 53, 541, arXiv: 1501.05317 ISBN: 10.1146/annurev-astro-082214-122348
- Bredehöft, J. H. 2020, *Frontiers in Astronomy and Space Sciences*, 7, 33
- Caracciolo, A., Lu, D., Balucani, N., et al. 2018, *The Journal of Physical Chemistry Letters*, 9, 1229
- Clark, T., Chandrasekhar, J., Spitznagel, G. W., & Schleyer, P. V. R. 1983, *J. Comput. Chem.*, 4, 294
- Ditchfield, R., Hehre, W. J., & Pople, J. A. 1971, *J. Chem. Phys.*, 54, 724
- Duflot, D., Toubin, C., & Monnerville, M. 2021, *Frontiers in Astronomy and Space Sciences*, 8, 24
- Dulieu, F., Amiaud, L., Congiu, E., et al. 2010, *Astronomy and Astrophysics*, 512, A30, arXiv: 0903.3120
- Eckart, C. 1930, *Physical Review*, 35, 1303
- Enrique-Romero, J., Ceccarelli, C., Rimola, A., et al. 2021, *Astronomy & Astrophysics*, 655, A9
- Enrique-Romero, J., Rimola, A., Ceccarelli, C., et al. 2022, *The Astrophysical Journal Supplement Series*, 259, 39
- Ferrari, B., Molpeceres, G., & T., L. 2023, *ACS: Earth and Space Science*
- Ferrero, S., Pantaleone, S., Ceccarelli, C., et al. 2023, *The Astrophysical Journal*, 944, 142
- Ferrero, S., Zamirri, L., Ceccarelli, C., et al. 2020, *ApJ*, 904, 11, arXiv: 2009.09763
- Frisch, M. J., Trucks, G. W., Schlegel, H. B., et al. 2016, *Gaussian16 Revision C.01*, pages: Gaussian 16, Revision C.01, Gaussian, Inc., Wallin
- Frost, M. J., Sharkey, P., & Smith, I. W. 1991, *Faraday Discussions of the Chemical Society*, 91, 305, publisher: The Royal Society of Chemistry
- Fuchs, G. W., Cuppen, H. M., Ioppolo, S., et al. 2009, *Astronomy and Astrophysics*, 505, 629
- Garrod, R. T. & Pauly, T. 2011, *Astrophysical Journal*, 735, 15, arXiv: 1106.0540 Publisher: American Astronomical Society
- Georgievskii, Y., Miller, J. A., Burke, M. P., & Klippenstein, S. J. 2013, *Journal of Physical Chemistry A*, 117, 12146
- Goerigk, L., Hansen, A., Bauer, C., et al. 2017, *Physical Chemistry Chemical Physics*, 19, 32184, publisher: The Royal Society of Chemistry
- Grimme, S., Antony, J., Ehrlich, S., & Krieg, H. 2010, *Journal of Chemical Physics*, 132, 154104
- Grimme, S., Ehrlich, S., & Goerigk, L. 2011, *Journal of Computational Chemistry*, 32, 1456, publisher: John Wiley & Sons, Ltd
- Guo, Y., Riplinger, C., Becker, U., et al. 2018, *The Journal of Chemical Physics*, 148, 011101
- Gutiérrez-Quintanilla, A., Layssac, Y., Butscher, T., et al. 2021, *MNRAS*, 506, 3734
- Hariharan, P. C. & Pople, J. A. 1973, *Theor. Chim. Acta*, 28, 213
- Hehre, W. J., Ditchfield, R., & Pople, J. A. 1972, *J. Chem. Phys.*, 56, 2257
- Helgaker, T., Klopper, W., Koch, H., & Noga, J. 1997, *The Journal of Chemical Physics*, 106, 9639
- Ioppolo, S., Cuppen, H. M., Romanzin, C., Van Dishoeck, E. F., & Linnartz, H. 2008, *The Astrophysical Journal*, 686, 1474
- Ioppolo, S., van Boheemen, Y., Cuppen, H. M., van Dishoeck, E. F., & Linnartz, H. 2011, *Monthly Notices of the Royal Astronomical Society*, 413, 2281
- Johnston, H. S. & Heicklen, J. 1962, *The Journal of Physical Chemistry*, 66, 532
- Lamberts, T., Cuppen, H. M., Fedoseev, G., et al. 2014, *Astronomy and Astrophysics*, 570, A57, arXiv: 1409.3055 Publisher: EDP Sciences
- Lamberts, T., Cuppen, H. M., Ioppolo, S., & Linnartz, H. 2013, *Physical Chemistry Chemical Physics*, 15, 8287, publisher: Royal Society of Chemistry
- Li, J., Chen, J., Zhang, D. H., & Guo, H. 2014, *The Journal of Chemical Physics*, 140, 044327
- Ma, J., Li, J., & Guo, H. 2012, *The Journal of Physical Chemistry Letters*, 3, 2482
- Martínez, L., Andrade, R., Birgin, E. G., & Martínez, J. M. 2009, *Journal of Computational Chemistry*, 30, 2157
- Masunov, A. E., Wait, E. E., & Vasu, S. S. 2018, *The Journal of Physical Chemistry A*, 122, 6355
- McClure, M. K., Rocha, W. R. M., Pontoppidan, K. M., et al. 2023, *Nature Astronomy* [arXiv:2301.09140]
- Meisner, J., Lamberts, T., & Kästner, J. 2017, *ACS Earth and Space Chemistry*, 1, 399, arXiv: 1708.05559 Publisher: American Chemical Society
- Minissale, M., Congiu, E., Manicò, G., Pirronello, V., & Dulieu, F. 2013, *Astronomy & Astrophysics*, 559, A49
- Molpeceres, G., Rimola, A., Ceccarelli, C., et al. 2019, *Monthly Notices of the Royal Astronomical Society*, 482, 5389
- Molpeceres, G., Rivilla, V. M., Furuya, K., et al. 2023a, *Monthly Notices of the Royal Astronomical Society*, 521, 6061
- Molpeceres, G., Zaverkin, V., Furuya, K., Aikawa, Y., & Kästner, J. 2023b, *Astronomy & Astrophysics*, 673, A51
- Molpeceres, G., Jiménez-Serra, I., Oba, Y., et al. 2022, *A&A*, 663, A41
- Neese, F. 2012, *WIREs Computational Molecular Science*, 2, 73, publisher: John Wiley & Sons, Ltd
- Neese, F. 2022, *WIREs Computational Molecular Science*, 12
- Neese, F. & Valeev, E. F. 2011, *Journal of Chemical Theory and Computation*, 7, 33
- Neese, F., Wennmohs, F., Becker, U., & Riplinger, C. 2020, *Journal of Chemical Physics*, 152, 224108
- Noble, J. A., Dulieu, F., Congiu, E., & Fraser, H. J. 2011, *The Astrophysical Journal*, 735, 121
- Oba, Y., Watanabe, N., Kouchi, A., Hama, T., & Pirronello, V. 2010a, *The Astrophysical Journal*, 712, L174
- Oba, Y., Watanabe, N., Kouchi, A., Hama, T., & Pirronello, V. 2010b, *The Astrophysical Journal*, 722, 1598
- Öberg, K. I., Boogert, A. C. A., Pontoppidan, K. M., et al. 2011, *ApJ*, 740, 109
- Pantaleone, S., Enrique-Romero, J., Ceccarelli, C., et al. 2021, *The Astrophysical Journal*, 917, 49, publisher: American Astronomical Society
- Pantaleone, S., Enrique-Romero, J., Ceccarelli, C., et al. 2020, *The Astrophysical Journal*, 897, 56, arXiv: 2004.11758 Publisher: American Astronomical Society
- Pauly, T. & Garrod, R. T. 2018, *The Astrophysical Journal*, 854, 13
- Perrero, J., Enrique-Romero, J., Martínez-Bachs, B., et al. 2022, *ACS Earth and Space Chemistry*, 6, 496
- Qasim, D., Lamberts, T., He, J., et al. 2019, *Astronomy and Astrophysics*, 626, A118, arXiv: 1905.06767
- Rimola, A., Skouteris, D., Balucani, N., et al. 2018, *ACS Earth and Space Chemistry*, 2, 720
- Rimola, A., Taquet, V., Ugliengo, P., Balucani, N., & Ceccarelli, C. 2014, *Astronomy and Astrophysics*, 572
- Riplinger, C., Pinski, P., Becker, U., Valeev, E. F., & Neese, F. 2016, *The Journal of Chemical Physics*, 144, 024109
- Snow, T. P. & McCall, B. J. 2006, *Annual Review of Astronomy and Astrophysics*, 44, 367, publisher: Annual Reviews ISBN: 0824309448
- Tachikawa, H. 2021, *ACS Omega*, 6, 16688
- Terwisscha van Scheltinga, J., Ligterink, N. F. W., Bosman, A. D., Hogerheijde, M. R., & Linnartz, H. 2022, *Astronomy & Astrophysics*, 666, A35
- Upadhyay, M., Pezzella, M., & Meuwly, M. 2021, *Journal of Physical Chemistry Letters*, 12, 6781
- Watanabe, N. & Kouchi, A. 2002, *The Astrophysical Journal*, 571, L173, publisher: IOP Publishing
- Woon, D. E. & Dunning, T. H. 1993, *The Journal of Chemical Physics*, 98, 1358
- Yu, H. S., He, X., Li, S. L., & Truhlar, D. G. 2016, *Chemical Science*, 7, 5032, publisher: The Royal Society of Chemistry
- Zhong, S., Barnes, E. C., & Petersson, G. A. 2008, *The Journal of Chemical Physics*, 129, 184116

Table A.1. Comparison of the potential energy reaction profile (e.g. no zero-point energy corrected) between our computational method and the high accuracy studies of Ma et al. (2012). The energy convention follows the same as in the preceding paper, considering the origin of energies in the deepest well of the PES (t-HOCO). All values are presented in kcal mol⁻¹

Structure	ΔE (This Work)	ΔE (Ma et al. (2012))
OH + CO	28.3	29.6
PRC	26.2	27.3
PRC'	27.4	28.4
TS1	28.6	29.0
TS1'	32.5	32.7
t-HOCO	0.0	0.0
TS2	9.4	9.3
c-HOCO	2.0	1.8
TS4	33.1	32.0
TS5	38.4	38.4
HCO ₂	34.7	16.8
TS6	22.1	20.9
CO ₂ + H	8.0	7.0

Appendix A: Gas-phase comparison with Ma et al. (2012)

We compare our energetics of the $\text{CO} + \text{OH} \longrightarrow \text{CO}_2 + \text{H}$ gas-phase reaction profile at the DLPNO-CCSD(T)/CBS//MN15-D3BJ/6-31+G(d,p) level with the high-quality CCSD(T)/AVTZ results presented in Ma et al. (2012) in Table A.1. Note that the energies presented here are not ZPVE corrected, unlike in the main manuscript. We observe excellent (between 0.0–1.3 kcal mol⁻¹) deviations between methods, e.g. chemical accuracy, for all structures except HCO₂. As we introduced in the methods section, this intermediate and the associated entrance and exit transition states, TS5 and TS6, are irrelevant to the reaction kinetics or dynamics (Ma et al. 2012; Masunov et al. 2018). Hence, a wrong prediction of the energetics of this intermediate does not affect our results, and we do not include it in our kinetic simulations. Yet, it is interesting to mention the reason for the discrepancy.

In Ma et al. (2012), the authors show that the HCO₂ intermediate belongs to the C_{2v} symmetry point group at the CCSD(T)/AVTZ level of theory. However, the geometries at the MN15-D3BJ/6-31+G(d,p) level converge to a C_s intermediate. The T₁ diagnostic at the DLPNO-CCSD(T)/cc-pVTZ level of theory for the HCO₂ intermediate hints at a strong multireference character (T₁=0.068), so it is not clear if the CCSD(T) or the MN15-D3BJ calculations are better in predicting the correct HCO₂ geometry. However, it is clear that a dual-level approach like DLPNO-CCSD(T)/CBS//MN15-D3BJ/6-31+G(d,p) will fail due to the mismatch of geometries. Despite the discrepancy found for HCO₂, the excellent agreement for all the relevant parts of the PES indicate that the studies on the H₂O and CO clusters will yield the correct energetics for the system.